Electronic absorption spectra of Cu^{2+} in MgO: *Ab initio* theory and experiment

José Luis Pascual*
Departamento de Química Física Aplicada, C-14, Universidad Autónoma de Madrid, 28049 Madrid, Spain

B. Savoini and R. González
Departamento de Física, Universidad Carlos III de Madrid, Avenida Universidad 30, 28911 Leganés, Madrid, Spain
(Received 23 March 2004; published 23 July 2004)

Ab initio model potential embedded cluster calculations on $(CuO_6)^{10-}$ units were used to model the electronic absorption spectra of Cu^{2+} doped MgO single crystals. These theoretical results were compared with optical absorption spectra determined experimentally. The major interactions present in the system, including intracluster electron correlation and scalar relativistic effects, were incorporated, providing a good description of both ground and excited states. The first step in calculating the electronic spectrum was to optimize the geometry of the cluster by taking into account the distortion produced by the Jahn-Teller effect. As a result a D_{4h} geometry was obtained, which is associated with a compression of the original octahedron along the *z* axis. Comparison of this geometry with extended x-ray absorption fine structure measurements is satisfactory. In clusters with D_{4h} geometry, vertical absorptions were calculated for *d-d* transitions as well as for ligand-to-metal charge transfer transitions. Optical absorption measurements showed two broad absorption bands at about 4.5 and 5.5 eV, which are attributed to charge-transfer transitions from the main ligand $2p\ t_{1u}\ \sigma$ and π molecular orbitals to the metal $3d$ shell.

DOI: 10.1103/PhysRevB.70.045109 PACS number(s): 71.55.−i, 31.15.−p, 78.40.Ha

I. INTRODUCTION

Magnesium oxide has been widely investigated for decades and continues to be of great research interest (see Ref. 1 and references therein), especially in relation to catalysis and its use as a ceramic material. The type, site distribution and oxidation state of the dopant ions strongly influence the properties of materials. The electronic properties and geometrical structure of the different dopant ions are variables of interest. Extensive work has been done on the characterization of the optical absorption bands induced in MgO by transition metal ions replacing the Mg^{2+} ions.[2–8] However, in Cu-doped MgO crystals, most investigations concentrate on the Jahn-Teller effect experienced by substitutional Cu^{2+} ions,[9–12] and information about the electronic transitions responsible for the optical absorption bands induced by Cu^{2+} ions has not been provided.

We have previously made a theoretical investigation of the Jahn-Teller (JT) effect on Cu^{2+} ions.[13] The emphasis was put on the JT distortion and not on the electronic spectrum, and consequently the wave function used was appropriate mainly for geometry optimization. In the present work, the calculation was extended to describe adequately the electronic spectrum. Wave functions that account for the major effects (electron correlation, lattice distortion, and relativistic effects) present in the system were used, following an approach that has been shown to be successful in similar applications.[14]

In addition, optical absorption spectra were measured in as-grown MgO:Cu single crystals and after reduction and oxidation at elevated temperatures. These spectra give information on the visible-ultraviolet (V-UV) region of the spectrum and are probably associated with ligand-to-metal charge transfer (CT) electronic transitions. These types of transitions have been addressed previously in ionic materials with theoretical techniques[15] similar to the ones used here, and a good agreement with experimental results has been obtained. Two broad absorption bands related to Cu^{2+} ions were observed at about 4.5 and 5.5 eV. Based on the theoretical calculations, these bands were assigned to different electronic transitions.

In Sec. II we provide a brief overview of the method together with a description of the calculations. Theoretical results for geometries and the electronic spectrum are discussed in Sec. III. Experimental results are presented in Sec. IV and compared with theoretical data in Sec. V. Conclusions are summarized in Sec. VI.

II. METHOD AND DETAILS OF THE CALCULATIONS

In MgO crystals, the optical spectrum of the defect center formed when Cu^{2+} ions substitute for Mg^{2+} ions is related to transitions localized in the $(CuO_6)^{10-}$ unit, which are supposed to be governed by bonding interactions between the impurity Cu^{2+} ion and its nearest O^{2-} neighbors. These interactions can be adequately described by applying to the $(CuO_6)^{10-}$ cluster standard high quality quantum mechanical methods, such as complete active space self consistent field (CASSCF)[16] and complete active space second-order perturbation theory (CASPT2)[17,18] calculations, which include dynamic electron correlation. In our calculations we incorporated relativistic effects by using the Cowan-Griffin (CG)-based effective core potential relativistic Hamiltonian CG-*ab initio* model potential (AIMP).[14,19] The effect of spin-orbit coupling was not considered.

The important embedding effect due to interactions with the rest of the components of the MgO host lattice was modeled by using the AIMP embedding technique.[14,20,21] The embedding model potentials are described in Sec. II A. The cal-

culations were performed with the MOLCAS-5 package.[22] The details of the embedded $(CuO_6)^{10-}$ cluster calculations are reported in Sec. II B.

A. Embedding potential

In the AIMP embedding technique used here, the one-electron terms of an isolated cluster Hamiltonian are corrected by adding the following embedding potential:

$$\sum_{\mu} [V_{\mu}^{lr-Coul}(i) + V_{\mu}^{sr-Coul}(i) + V_{\mu}^{exch}(i) + P_{\mu}(i)], \qquad (1)$$

where μ runs over the crystal ions (Mg^{2+}, O^{2-}), $V_{\mu}^{lr-Coul}(i)$ stands for the long-range Coulomb potential exerted by ion μ on the ith electron of the cluster (i.e., $\Sigma_{\mu} V_{\mu}^{lr-Coul}(i)$ is the Madelung potential of the lattice), $V_{\mu}^{sr-Coul}(i)$ stands for the potential that represents the deviation of the lattice ion from a point charge (the short-range Coulomb potential), $V_{\mu}^{exch}(i)$ is the exchange potential, and $P_{\mu}(i)$ is the orthogonality potential, which prevents the cluster wave function from collapsing into the lattice ion μ. Only the dynamic cluster/lattice correlation is excluded from the embedding potential. The detailed form of these potentials can be found in Refs. 20 and 23, together with the procedure that leads to their calculation using the lattice ions wave functions. In this work, the total-ion potentials were taken from Refs. 13 and 24.

Ideally, the AIMP embedding potential is built up by adding to the cluster Hamiltonian the AIMP total-ion potentials of all the lattice ions outside the cluster. In practice, the infinite sum is truncated as follows: we include the AIMP embedding potentials of all ions located within a cube of length 16.845 Å centered in the impurity site (722 ions) plus other 4184 ions, located in a cube surrounding the first one (length 33.690 Å), represented by point charges bearing the nominal ion charge, except those located at the frontier, which bear fractional charges according to Evjen's method.[25] In this way, we assure that the cluster embedding potential provides a good representation of the quantum effects as well as the long-range Madelung effects. In a first approximation, all these ions are located at the sites of a perfect unpolarized MgO lattice (NaCl lattice type, point group $O_h^5(Fm3m)$, $a_0 = 4.2112$ Å).[26]

The AIMP embedding method has been extended to include the polarization and relaxation of the lattice, represented by shell-model (SM) potentials, configuring the so-called AIMP/SM method.[21] In all the cases studied so far,[14,27] the effect of the lattice distortion on the cluster geometry in this type of noncharged impurity defect was to enhance the distortion by about 20–30% with respect to the perfect geometries. In the present work, we used the AIMP/SM method to check this effect. This method consists, basically, of an iterative series of embedded cluster-surrounding lattice relaxation calculations, so that, eventually, a geometrical configuration of the lattice is found to be consistent with the quantum-mechanical description of the cluster in a given electronic state.[21] The geometrical configuration of the lattice was consistent with the octahedral $a\ ^2E_g$ ground state and was used to calculate the Jahn-Teller parameters and excited state geometries, as well as the optical properties. This approximation is mainly suitable to calculate vertical absorption energies. In order to perform the AIMP/SM calculations, pair potentials as well as shell parameters are required for the MgO lattice. In the present work, we used the parameters of Ref. 28. The calculations performed at this AIMP/SM level are summarized in Tables I–III.

TABLE I. Unrelaxed lattice (AIMP) optimized O_h geometries and relaxed lattice (AIMP/SM) optimized O_h geometries, $\overline{\nu}_{a_{1g}}$ vibrational frequencies for the different electronic states of the $(CuO_6)^{10-}$ cluster, and minimum-to-minimum transition energies T_e from the $a\ ^2E_g$ ground state.[a]

State	R_0(Cu-O) (Å) AIMP	R_0(Cu-O) (Å) AIMP/SM	$\overline{\nu}_{a_{1g}}$ (cm^{-1})	T_e (eV)
$a\ ^2E_g$	2.153	2.170	574	0
$a\ ^2T_{2g}$	2.160	2.176	592	1.11
$a\ ^2T_{1u}$	2.233	2.249	603	4.20
$^2T_{2u}$	2.239	2.255	609	4.56
$^2T_{1g}$	2.237	2.253	600	4.80
$b\ ^2E_g$	2.241	2.257	613	4.90
$b\ ^2T_{2g}$	2.253	2.268	621	5.22
$b\ ^2T_{1u}$	2.251	2.266	621	5.52
$^2A_{1g}$	2.247	2.263	612	7.05

[a]For comparison, R_0(Mg-O) in undoped MgO is 2.106 Å.

B. The $(CuO_6)^{10-}$ defect cluster calculations

The calculations on the embedded cluster used a Cowan-Griffin relativistic effective core potential both for Cu^{2+} and O^{2-} ions. For Cu^{2+} we used a [Mg] core CG-AIMP taken from Ref. 29 together with the corresponding (9*s*5*p*5*d*) basis set, augmented with one *p* polarization function,[30] one *d* dif-

TABLE II. Equilibrium tetragonal geometries and Jahn-Teller $E \otimes e$ coupling parameters for the $a\ ^2E_g$ electronic state.

Octahedral structure	
R_0(Cu-O) (Å)	2.170
$\overline{\nu}_{a_{1g}}$ (cm^{-1})	574
2β (cm^{-1})	27
Elongated D_{4h} structure ($^2B_{1g}$ state)	
R_{ax}(Cu-O) (Å)	2.230
R_{eq}(Cu-O) (Å)	2.141
$\overline{\nu}_{e_{g,\theta}}$ (cm^{-1})	447
E_{JT} (cm^{-1})	468
Compressed D_{4h} structure ($^2A_{1g}$ state)	
R_{ax}(Cu-O) (Å)	2.107
R_{eq}(Cu-O) (Å)	2.202
$\overline{\nu}_{e_{g,\theta}}$ (cm^{-1})	419
E_{JT} (cm^{-1})	495
$E_{JT}/\overline{\nu}_{e_{g,\theta}}$	1.18
$\overline{\nu}_{e_{g,\theta}}/\lvert 2\beta \rvert$	15.5

TABLE III. Calculated vertical transition energies for each symmetry between the minimum of the ground state and the different excited electronic states and oscillator strengths for the $g \rightarrow u$ transitions. Available experimental results are also shown.

		O_h energy (eV)	f		D_{4h} compressed energy (eV)	f		D_{4h} elongated energy (eV)	f	Experimental energy (eV)	f [b]
Ground state d-d transitions	$a\,^2E_g \rightarrow$	⋯	⋯	$^2A_{1g} \rightarrow$	⋯	⋯	$^2B_{1g} \rightarrow$	⋯	⋯	⋯	⋯
		⋯	⋯	$^2B_{1g}$	0.25	⋯	$^2A_{1g}$	0.23	⋯	⋯	⋯
	$a\,^2T_{2g}$	1.11	⋯	^2E_g	1.21	⋯	$^2B_{2g}$	1.18	⋯	1.24[a]	⋯
		⋯	⋯	$^2B_{2g}$	1.29	⋯	^2E_g	1.25	⋯	1.39[a]	⋯
CT transitions	$a\,^2T_{1u}$	4.58	0.1042	^2E_u	4.69	0.0425	$^2A_{2u}$	4.67	>0.0001	4.5[b], 4.52[a]	0.13
				$^2A_{2u}$	4.73	0.0628	^2E_u	4.71	0.1059	⋯	⋯
	$^2T_{2u}$	5.01	0.0001	$^2B_{2u}$	5.10	>0.0001	^2E_u	5.11	0.0011	⋯	⋯
				^2E_u	5.14	0.0006	$^2B_{2u}$	5.14	0.0001	⋯	⋯
	$^2T_{1g}$	5.22	⋯	$^2A_{2g}$	5.34	⋯	^2E_g	5.34	⋯	⋯	⋯
				^2E_g	5.35	⋯	$^2A_{2g}$	5.34	⋯	⋯	⋯
	$b\,^2E_g$	5.47	⋯	$^2A_{1g}$	5.45	⋯	$^2B_{1g}$	5.45	⋯	⋯	⋯
				$^2B_{1g}$	5.54	⋯	$^2A_{1g}$	5.55	⋯	⋯	⋯
	$b\,^2T_{2g}$	5.84	⋯	$^2B_{2g}$	5.87	⋯	^2E_g	5.93	⋯	⋯	⋯
				^2E_g	6.04	⋯	$^2B_{2g}$	6.06	⋯	⋯	⋯
	$b\,^2T_{1u}$	6.11	0.0818	^2E_u	6.25	0.0285	$^2A_{2u}$	6.21	>0.0001	5.5[b]	0.19
				$^2A_{2u}$	6.28	0.0644	^2E_u	6.26	0.0920	⋯	⋯
	$^2A_{1g}$	7.60	⋯	$^2A_{1g}$	7.74	⋯	$^2A_{1g}$	7.73	⋯	⋯	⋯

[a]Reference 37, see text for details.
[b]This work.

fuse function,[31] and three f-type functions,[32] finally contracted as $[3s3p5d1f]$. For O^{2-}, we used a [He] core CG-AIMP and the $(5s5p)$ valence basis set of Ref. 29, augmented with a diffuse p function for the anion[33] and one d polarization function,[30] and contracted as $[2s3p1d]$. Following Ref. 13, extra orthogonalization functions were used for the (100)-second neighboring Mg^{2+} ions. These functions are the $(10s4p)$ basis set used for Mg^{2+} on the $MgO:Mg^{2+}$ embedded ion calculations,[13] totally contracted as $[1s1p]$. The total number of basis set functions is 159.

In order to obtain the geometry and electronic spectrum of $MgO:Cu^{2+}$, relativistic calculations were performed using the spin-free Hamiltonian for $(CuO_6)^{10-}$ embedded in the AIMP representation of the MgO lattice described in Sec. II A. First, we performed CASSCF calculations,[16] incorporating 45 active electrons in the mainly Cu $3d$ and O $2p$ molecular orbitals. Second, these wave functions were taken as the zeroth order wave functions for subsequent second order perturbation theory calculations (CASPT2)[17] using the multistate version of this method (MS-CASPT2).[18] A total of 63 electrons occupying the Cu $3p$, $3d$ and O $2s$, $2p$ molecular orbitals were correlated. For all the distances studied, the CASPT2 wave functions showed good behavior: large and uniform weight of the zeroth order wave function (around 70% and always larger than 68%) and no sign of intruder states. The results presented in this paper refer to this CASPT2 level of calculation.

We studied the states originating at the Cu $3d^9$ configuration, ^2E_g and $^2T_{2g}$, as well as the states induced by the transfer of one electron from the O $2p$ shell to the Cu $3d$ shell, which will be referred to as CT states.

III. THEORETICAL RESULTS

A. Cluster geometries

The potential energy curves for the ground and lowest excited states as a function of the Cu-O distance are plotted in Fig. 1. An optimization of the geometry of the $(CuO_6)^{10-}$ cluster in these states was made. We optimized the Cu-O distance, R_0, of the $(CuO_6)^{10-}$ unit restricted to O_h symmetry, and calculated the breathing mode vibrational frequencies, $\overline{\nu}_{a_{1g}}$. These results together with the calculated minimum-to-minimum transition energies, T_e, from the $a\,^2E_g$ ground state are summarized in Table I. Since the vibrational frequencies are similar for the different electronic states, these numbers should be close to the zero-phonon absorption transitions. In Table I, the Cu-O distances are for all the states larger than the Mg-O distance in the perfect lattice, 2.106 Å, consistent with the slight distortion induced by the larger ionic radius of Cu^{2+} ions compared to Mg^{2+} ions.[34] The data in Table I show that the effect of lattice relaxation is an enhancement of the distortion with respect to the perfect MgO lattice. For the $a\,^2E_g$ ground state this extra distortion is 0.017 Å, and is almost the same for the rest of the states (0.015–0.016 Å).

The equilibrium distances for the different states correlate well with the electronic configuration. The $a\,^2E_g$ ground state belongs to the $t_{2g}^6 e_g^3$ configuration, and the first excited

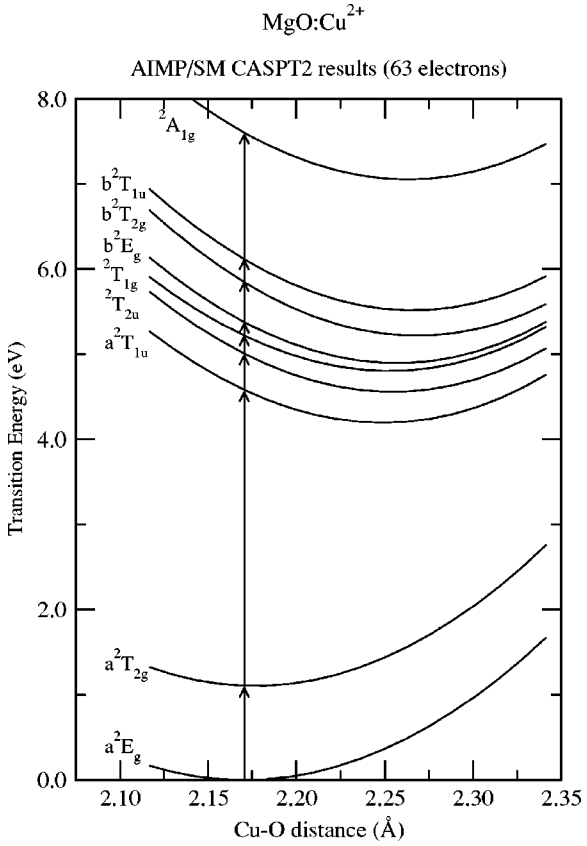

FIG. 1. Potential energy curves of the ground and lowest excited states of the $(CuO_6)^{10-}$ cluster as a function of the Cu-O distance in the a_{1g} vibrational mode (O_h symmetry). Arrows mark the vertical transitions from the ground state.

state, $a\ ^2T_{2g}$, belongs to the so-called 10 Dq transition, with a $t_{2g}^5 e_g^4$ configuration. The transition from the t_{2g} to the e_g orbital weakens the Cu-O bonding interactions, and as a result the Cu-O distance is larger in the $a\ ^2T_{2g}$ excited state. In the charge transfer states, an electron from the O $2p$ shell (in O_h symmetry, these atomic orbitals transform according to the a_{1g}, e_g, t_{1g}, t_{2g}, t_{1u} (2) and t_{2u} irreducible representations) occupies the antibonding Cu e_g orbital, giving rise to the following electronic states: $^2A_{1g}$, $b\ ^2E_g$, $^2T_{1g}$, $b\ ^2T_{2g}$, $a\ ^2T_{1u}$, $b\ ^2T_{1u}$, and $^2T_{2u}$. Hence, the equilibrium distance is larger for these charge transfer states than for the ground state.

Degenerate electronic states in cubic environments are Jahn-Teller unstable and the coupling with nontotally symmetric vibrational modes removes their degeneracy. This effect is crucial for the interpretation of the spectra of d^9 impurity ions, thus, the geometry of the cluster in its ground state was reoptimized. Starting with the O_h equilibrium geometry and the embedded-cluster energy we calculated the Jahn-Teller coupling of the $a\ ^2E_g$ state with the doubly degenerate e_g vibrational mode of the $(CuO_6)^{10-}$ cluster ($E \otimes e$ coupling). Minimizing with respect to the $e_{g,\theta}$ normal coordinate and neglecting the coupling with triply degenerate t_{2g} modes lead to tetragonal (D_{4h} symmetry) compressed/elongated geometries.[35]

Table II displays the optimized geometries and the $e_{g,\theta}$ vibrational frequency, $\overline{\nu}_{e_{g,\theta}}$, for both the compressed and the elongated structures together with the Jahn-Teller stabilization energy, E_{JT}, and the $E_{JT}/\overline{\nu}_{e_{g,\theta}}$ ratio for the most stable state: the compressed structure. This last number is a measure of the strong/weak linear JT coupling.[35] We also give the values of the difference in energy, 2β, between the two structures defined as

$$2\beta = E_{JT}(\text{compressed}) - E_{JT}(\text{elongated}) \qquad (2)$$

and the ratio $\overline{\nu}_{e_{g,\theta}}/2\beta$ for the compressed configuration (the most stable one), which is a measure of the static/dynamic behavior within the strong linear JT coupling approximation. The most stable distortion is a compression along the z axis of a D_{4h} symmetry structure (actually, we have constrained the optimization to the D_{4h} symmetry; further relaxation to D_{2h} symmetry is expected to bring only a negligible extra distortion).[13] However, the barrier between the compressed and the elongated configurations is only 27 cm^{-1}, so the potential energy surface is very close to the "Mexican hat" shape, characteristic of pure linear JT ($E \otimes e$) coupling.[35] The dynamics of the cluster can be described as an almost free rotation among the three equivalent D_{4h} minima (i.e., compressions along the three symmetry axes), in what can be denoted as a dynamic JT effect (strong JT linear coupling but small barrier between minima).

This JT coupling has been previously studied[13] considering wave functions of SCF level, without dynamic correlation. These results were qualitatively similar to the ones discussed here regarding the sign of the distortion and the dynamics of the cluster, but incorporation of the electron correlation results in a larger JT energy (495 versus 335 cm^{-1}),[13] indicating a somewhat stronger JT linear coupling. As has been pointed out in Ref. 13, those results provide dynamics that are systematically less static than that obtained experimentally. The inclusion of dynamic correlation means a step towards a more static picture. This result concurs with calculations[36] on $[Cu(H_2O)_6]^{2+}$.

The equilibrium geometry has been investigated[1] by extended x-ray absorption fine structure (EXAFS) on polycrystalline MgO:Cu, with a dopant concentration of about 5.2%. It has been concluded that an undisturbed $(CuO_6)^{10-}$ unit with R_0(Cu-O)=2.104 Å is the most plausible representation of the first coordination sphere, however, a distortion in which the difference between the equatorial, R_{eq}, and axial, R_{ax}, Cu-O distances is less than 0.11 Å cannot be ruled out.[1] For the compressed D_{4h} structure, our calculated difference is 0.095 Å, compatible with the EXAFS data. Taking into account the dynamic behavior of the cluster, the calculated structure can be represented as an octahedral unit, with an average distance of 2.170 Å. This distance is about 0.07 Å larger than that obtained in the EXAFS experiments. The distance between a Cu^{2+} ion and the second neighboring Mg^{2+} ions was found to be R_1(Cu-Mg)=2.969±0.010 Å in the EXAFS experiments,[1] indicating that the lattice is essentially undistorted since the distance between two Mg^{2+} second neighboring ions in pure MgO, R_1(Mg-Mg), is 2.978 Å. In the present study, we find a slight outwards distortion, with R_1(Cu-Mg)=3.001 Å.

To our knowledge, no direct experimental determination of the vibrational frequencies or the Jahn-Teller stabilization energies exist.

B. Electronic transitions

Table III shows the vertical transition energies between the minimum of the ground state and the different electronic states for both O_h and D_{4h} symmetries. These transitions are represented by arrows in Fig. 1. Vertical transition parameters are also given for elongated and compressed D_{4h} conditions, with an energy barrier between them of only 27 cm^{-1}, as discussed in Sec. III A. Excitation energies and oscillator strengths for the three CT $g \rightarrow u$ transitions, which are spin and symmetry allowed in O_h symmetry, are also given in Table III.

According to our calculations, and taking into account the selection rules for the transitions, three CT transitions should be allowed and should have significant intensities in the spectrum. However, in Table III the values of the oscillator strengths for the transitions to the $a\ ^2T_{1u}$ and $b\ ^2T_{1u}$ states are at least 2 orders of magnitude larger than the transitions to the $^2T_{2u}$ state. Thus, only two main transitions should yield absorption bands with maxima at about 4.7 and 6.2 eV, respectively. Since the equilibrium distances of the final states, $a\ ^2T_{1u}$ and b^2T_{1u}, are appreciably different from that of the $a\ ^2E_g$ ground state (Table I), these bands should be broad.

IV. EXPERIMENTAL RESULTS

Copper-doped MgO single crystals were grown at the Oak Ridge National Laboratory by an arc fusion technique.[38] The dopant was added to the melt in the form of CuO. The resulting MgO crystals were colorless in appearence. The concentration of copper was determined by neutron activation analysis to be ≈36 ppm.[39]

Optical absorption measurements in the UV-VIS-IR region were made with a Perkin-Elmer, Lambda 19 spectrophotometer. Oxidation of the samples at elevated temperatures was performed in flowing oxygen with the samples placed in a platinum basket inside an alumina tube inserted in a horizontal furnace.

A. Optical absorption measurements

Copper may exist in more than one valence state like many of the transition metal ions. In MgO, it exists chiefly as Cu^{2+}, Cu^{+}, or metallic Cu^0. Figure 2 (middle) shows the optical-absorption spectrum of an as-grown $MgO:Cu^{2+}$ crystal. Two absorption bands of about equal intensity are observed at ≈5.5 and 4.5 eV with a full width at half maxima (FWHMs) of ≈0.7 and 0.5 eV, respectively, in agreement with previous findings.[40] Thermochemical reduction (TCR) at about 1800 K for 30 min induces a dramatic decrease in the intensity of these two bands and a shift of the high energy band to 5.3 eV (FWHM ≈0.6 eV). These observations suggest that the 5.5 eV band is a composed band and that the lower energy side diminishes disproportionally more slowly. In addition, TCR results in the emergence of a very broad extinction band at ≈3.0 eV, which has been previously associated with the formation of metallic copper nanocolloids.[40] Subsequent oxidation at ≈1850 K for 80 min anneals out the colloids. Furthermore, the measured intensities of the 5.5 and 4.5 eV bands are much higher than those determined in the as-grown sample, with the 5.5 eV band increasing disproportionally more rapidly; their FWHMs are 1.0 and 0.7 eV, respectively. These results clearly show that: (1) these two bands are due to electronic transitions of Cu^{2+} ions and (2) in the as-grown sample most of the copper ions are not double ionized, which is not surprising since the crystals were grown in a reducing atmosphere.

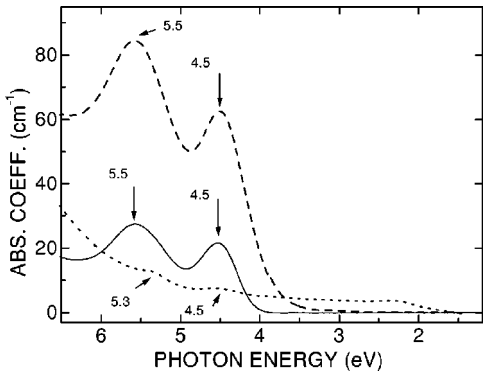

FIG. 2. Optical absorption spectra of an as-grown MgO:Cu crystal (solid line), after TCR (dotted line) and after subsequent oxidation (dashed line).

The oscillator strengths of the Cu^{2+} absorption bands were calculated using Smakula's equation (as modified by Dexter[41]) for Gaussian bands

$$f = \frac{8.21 \times 10^{16}}{N} \frac{n}{(n^2+2)^2} \int \alpha(E) d\overline{E}, \tag{3}$$

where N is the ion density in ions/cm^3, n is the refractive index at each band peak, α is the absorption coefficient in cm^{-1}, and E is the photon energy in eV.

Assuming that in the oxidized crystal almost all the copper in the sample is dissolved as substitutional Cu^{2+} ions, the resulting value for N is $1.8 \times 10^{18} cm^{-3}$, which yields 0.19 and 0.13 for the oscillator strengths of the 5.5 and 4.5 eV bands, respectively. These results are in reasonable agreement with those found in our calculations (Table III), given that the 0.19 value may be overestimated, as the behavior of these two bands under reducing and oxidizing treatments indicates.

V. DISCUSSION

In this section, theoretical results are compared with optical absorption measurements. While there is a relatively large amount of information concerning the electron paramagnetic resonance spectrum of Cu-doped MgO,[9–12] little is known about its optical absorption. The present work is a study of the optical absorption spectrum in the CT region of $MgO:Cu^{2+}$ single crystals.

The IR absorption spectrum of complexes where the Cu^{2+} ion is coordinated with six oxygen ions has been more ex-

tensively studied (see Ref. 42 and references therein). The IR bands were generally attributed to $d-d$ transitions between states in a distorted octahedron with symmetry D_{4h} or D_{2h}. Usually, the distortion is supposed to be an elongation in the z-axis direction, contrary to our results in Sec. III A. Three $d-d$ bands (or four in D_{2h} symmetry) are usually resolved in the IR spectrum, with maxima at about 0.99 eV (8000 cm^{-1}), 1.24 eV (10 000 cm^{-1}), and 1.55 eV (12 500 cm^{-1}) (see, for example, Ref. 43). The first band has been assigned to the $^2B_{1g} \rightarrow {}^2A_{1g}$ transition (elongated octahedron D_{4h} symmetry), and the two latter bands have been associated with transitions from the $^2B_{1g}$ ground state to the $^2B_{2g}$ and ^2E_g states,[43] respectively, both states related to the $a\ ^2T_{2g}$ state (O_h symmetry).

In reflectance experiments on MgO-CuO solutions with concentrations of the dopant larger than 1%, four absorption bands at 0.57, 0.69, 0.99, and 1.39 eV were observed; in addition, two shoulders at 1.24 and 1.86 eV were resolved.[37] Our calculations show that two close-lying electronic transitions occur at 1.21 and 1.29 eV; these transitions are from the $^2A_{1g}$ ground state to the ^2E_g, $^2B_{2g}$ states, respectively, originating at the octahedral $a\ ^2T_{2g}$ state (Table III). We tentatively assign the shoulder at 1.24 eV and the broadband at 1.39 eV, both observed in the absorption spectrum to these two transitions (the departure between the experimental and theoretical energies is on the order of 0.10 eV). The results of Table III indicate that another band at about 0.25 eV, related to the $^2A_{1g} \rightarrow {}^2B_{1g}$ transition, should also be observed in the IR region of the spectrum, but this low energy range was not measured.[37] We cannot assign the other bands observed in the absorption spectrum of Ref. 37. The three bands at 0.57, 0.69, and 0.99 eV might be tentatively related to the bands resolved around 1.0 eV in hexacoordinated copper compounds.[42,43] However, these bands must not be due to the transition between the two lowest levels induced by the JT splitting of the $a\ ^2E_g$ octahedral level, since the energy of this transition is 0.25 eV according to our calculations. Furthermore, this transition energy is,[35] in a first approximation, equal to $4E_{JT}$, thus a value of 1 eV yields 2000 cm^{-1} for E_{JT} which we estimate is unrealistically high. A very large JT tetragonal distortion would explain this very large E_{JT} value, but the EXAFS results show that the $(CuO_6)^{10-}$ unit can only be slightly distorted.[1] It should be noted, however, that the high degree of doping in the polycrystalline samples used in the EXAFS experiments makes the comparison with our theoretical results difficult.

A more straightforward comparison of the calculations can be made with the optical absorption measurements in the UV-VIS range presented in Sec. IV, since they were made in MgO single crystals with a small amount of doping. The 4.5 eV band observed in the optical absorption spectrum of Fig. 2 and in the spectrum of Ref. 37 can be confidently assigned to the $a\ ^2E_g \rightarrow a\ ^2T_{1u}$ transition based on the energy position of the band (Table III), and the fact that it is an allowed transition. On intensity grounds, the band at 5.5 eV (Fig. 2) might be assigned to the $a\ ^2E_g \rightarrow b\ ^2T_{1u}$ transition. The difference in energy with the calculated transition is larger in this case and around 0.7 eV (13%). The calculated oscillator strengths (Table III) are similar for the two transitions discussed here, in agreement with the experimental observation (Fig. 2) also of similar intensity for both bands. The oscillator strength of the $a\ ^2E_g \rightarrow {}^2T_{2u}$ transition is at least 2 orders of magnitude smaller than those of the $a\ ^2E_g \rightarrow a\ ^2T_{1u}$ and $a\ ^2E_g \rightarrow b\ ^2T_{1u}$ transitions, consequently, the associated band is not resolved in the absorption spectrum of Fig. 2. Absorption bands were not resolved in the IR, even in a sample with a thickness of 15 mm, because the associated transitions are symmetry forbidden and the resulting small oscillator strengths preclude their detection, unless very heavily doped samples are used.

VI. CONCLUSIONS

Theoretical investigations of the electronic spectra of Cu-doped MgO single crystals using wave functions which include electron correlation, provide results for the CT transitions that are in agreement with the experimental data obtained from optical absorption measurements. MS-CASPT2 calculations based on CASSCF wave functions, which include Cu $3d$ and O $2p$ electrons as the active space, were used to determine the electron correlation. The distortion induced by the JT effect on the $(CuO_6)^{10-}$ cluster results in a D_{4h} geometry associated with compression along the z axis.

Two absorption bands at about 4.5 and 5.5 eV are attributed to charge-transfer transitions from the main ligand $2p$ t_{1u} σ and π molecular orbitals to the metal $3d$ shell. The resulting differences in energy of about 10% between theoretical and experimental data are reasonable. These differences may be due to an incomplete treatment of the electron correlation (probably nondynamic correlation), whose correction may imply the use of even larger zeroth order wave functions. These calculations are not currently possible due to computational limitations.

ACKNOWLEDGMENTS

The authors would like to acknowledge Dr. Luis Seijo (UAM, Madrid) for helpful discussions and suggestions and Dr. Yok Chen for providing the MgO:Cu crystals. This work was partly supported by MCyT of Spain (Dirección General de Investigación Project Nos. BQU2002-01316 and MAT2002-01870).

*Email address: joseluis.pascual@uam.es

[1] N. Hilbrandt and M. Martin, J. Phys. Chem. B **103**, 4797 (1999).
[2] R. W. Soshea, A. J. Dekker, and J. P. Sturtz, J. Phys. Chem. Solids **5**, 23 (1958).
[3] D. S. McClure, J. Chem. Phys. **36**, 2757 (1962).
[4] W. A. Sibley, J. L. Kolopus, and W. C. Mallard, Phys. Status Solidi **31**, 223 (1969).
[5] F. A. Modine, Phys. Rev. B **8**, 854 (1973).

[6] A. J. Mann and P. J. Stephens, Phys. Rev. B **9**, 863 (1974).
[7] M. V. Iverson, J. C. Windschief, and W. A. Sibley, Appl. Phys. Lett. **36**, 183 (1980).
[8] R. Llusar, M. Casarrubios, Z. Barandiarán, and L. Seijo, J. Chem. Phys. **105**, 5321 (1996).
[9] J. W. Orton, P. Auzins, J. H. E. Griffiths, and J. E. Wertz, Proc. Phys. Soc. London **78**, 554 (1961).
[10] U. Höchli, K. A. Müller, and P. Wysling, Phys. Lett. **15**, 5 (1965).
[11] K. Zdanský, Phys. Rev. **177**, 490 (1969).
[12] R. W. Reynolds, L. A. Boatner, M. M. Abraham, and Y. Chen, Phys. Rev. B **10**, 3802 (1974).
[13] J. L. Pascual, L. Seijo, and Z. Barandiarán, J. Chem. Phys. **98**, 9715 (1993).
[14] L. Seijo and Z. Barandiarán, in *Computational Chemistry: Reviews of Modern Trends*, edited by J. Leszczynski (World Scientific, Singapore, 1999), Vol. 4, p. 55.
[15] A. Al-Abdalla, L. Seijo, and Z. Barandiarán, J. Chem. Phys. **109**, 6396 (1998).
[16] B. O. Roos, P. R. Taylor, and P. E. M. Siegbahn, Chem. Phys. **48**, 157 (1980); P. E. M. Siegbahn, A. Heiberg, J. Almlöf, and B. O. Roos, J. Chem. Phys. **74**, 2384 (1981); P. Siegbahn, A. Heiberg, B. Roos, and B. Levy, Phys. Scr. **21**, 323 (1980).
[17] K. Andersson, P.-Å. Malmqvist, B. O. Roos, A. J. Sadlej, and K. Wolinski, J. Phys. Chem. **94**, 5483 (1990); K. Andersson, P.-Å. Malmqvist, and B. O. Roos, J. Chem. Phys. **96**, 1218 (1992).
[18] J. Finley, P.-Å. Malmqvist, B. O. Roos, and L. Serrano-Andrés, Chem. Phys. Lett. **288**, 299 (1998).
[19] L. Seijo, J. Chem. Phys. **102**, 8078 (1995).
[20] Z. Barandiarán and L. Seijo, J. Chem. Phys. **89**, 5739 (1988).
[21] J. L. Pascual and L. Seijo, J. Chem. Phys. **102**, 5368 (1995).
[22] K. Andersson, M. Barysz, A. Bernhardsson, M. R. A. Blomberg, D. L. Cooper, T. Fleig, M. P. Fülscher, C. de Graaf, B. A. Hess, G. Karlström, R. Lindh, P.-Å. Malmqvist, P. Neogrády, J. Olsen, B. O. Roos, B. Schimmelpfennig, M. Schütz, L. Seijo, L. Serrano-Andrés, P. E. M. Siegbahn, J. Stårling, T. Thorsteinsson, V. Veryazov, and P.-O. Widmark, MOLCAS (Lund University, Sweden, 2000), Version 5.
[23] Z. Barandiarán and L. Seijo, in *Studies in Physical and Theoretical Chemistry*, Computational Chemistry: Structure, Interactions and Reactivity, Vol. 77(B), edited by S. Fraga (Elsevier, Amsterdam, 1992), p. 435.
[24] M. Nygren, L. Pettersson, Z. Barandiarán, and L. Seijo, J. Chem. Phys. **100**, 2010 (1994).
[25] H. M. Evjen, Phys. Rev. **39**, 675 (1932).
[26] R. W. G. Wyckoff, *Crystal Structures* (Wiley, New York, 1963).
[27] J. L. Pascual, Phys. Rev. B **67**, 115112 (2003).
[28] M. J. L. Sangster and A. M. Stoneham, Philos. Mag. B **43**, 597 (1981).
[29] Z. Barandiarán and L. Seijo, Can. J. Chem. **70**, 409 (1992).
[30] J. Andzelm, M. Klobukowsky, E. Radzio-Andzelm, Y. Sakai, and H. Tatewaki, *Gaussian Basis Sets for Molecular Calculations* (Elsevier, Amsterdam, 1984).
[31] P. J. Hay, J. Chem. Phys. **66**, 4377 (1977).
[32] L. G. M. Pettersson (private communication).
[33] T. H. Dunning, Jr. and P. J. Hay, in *Modern Theoretical Chemistry*, edited by H. F. Schaeffer III (Plenum, New York, 1977).
[34] R. D. Shannon, Acta Crystallogr., Sect. B: Struct. Crystallogr. Cryst. Chem. **32**, 751 (1976).
[35] I. B. Bersuker, *The Jahn-Teller Effect and Vibronic Interactions in Modern Chemistry* (Plenum, New York, 1984).
[36] R. Åkesson, L. G. M. Pettersson, M. Sandström, and U. Wahlgren, J. Phys. Chem. **96**, 150 (1992).
[37] O. Schmitz-DuMont and H. Fendel, Monatsch. Chem. **96**, 495 (1965).
[38] M. M. Abraham, C. T. Butler, and Y. Chen, J. Chem. Phys. **55**, 3752 (1971).
[39] K. L. Tsang and Y. Chen, J. Appl. Phys. **54**, 4531 (1983).
[40] C. Ballesteros, R. González, and Y. Chen, Phys. Rev. B **37**, 8008 (1988).
[41] D. L. Dexter, in *Solid State Physics*, edited by F. Seitz and D. Turnbull (Academic, New York, 1968), Vol. 6, p. 370.
[42] A. B. P. Lever, *Inorganic Electronic Spectroscopy*, 2nd ed., Studies in Physical and Theoretical Chemistry, Vol. 33 (Elsevier, Amsterdam, 1984).
[43] M. A. Hitchman and T. D. Waite, Inorg. Chem. **15**, 2150 (1976).